Electronics and Communications in Japan, Vol. 93, No. 2, 2010
Translated from Denki Gakkai Ronbunshi, Vol. 127-C, No. 10, October 2007, pp. 1667–1672

Effect of External Tissue Resistivity on Threshold Level of Myelinated Nerve Fiber

TAKEHITO HAYAMI,[1] KEIJI IRAMINA,[2] and XIAN CHEN[1]
[1]Digital Medicine Initiative, Kyushu University, Japan
[2]Graduate School of Information Science and Electrical Engineering, Kyushu University, Japan

SUMMARY

The rise of the threshold of electric current stimulation to generate compound action potential of nerve conduction study is considered to have a relationship to malfunctions of the nerve. The effect of the decrease of the resistivity of the external tissue and the thickness of myelin sheaths was investigated by computer simulation. A myelinated human nerve fiber dipped in the homogeneous conductor was stimulated with a monopolar cathode located outside the axon. The rise of the threshold by demyelination was found to be comparable to the effect of the decrease of the resistivity of the external tissue by a few Ωm when the external resistivity is about 10 Ωm. Actually the reduction of the thickness of the myelin sheaths also reduces the resistivity of the external tissue. Therefore, the contribution of both effects in the case of demyelination was estimated. As a result, the contributions of each effect were antagonized. As one of the causes of the rise of the threshold of nerve activation, the decrease of the resistivity of the external tissue is considerable. © 2010 Wiley Periodicals, Inc. Electron Comm Jpn, 93(2): 50–56, 2010; Published online in Wiley InterScience (www.interscience.wiley.com). DOI 10.1002/ecj.10065

Key words: myelinated nerve; electric stimulation; neural function diagnosis.

1. Introduction

Nerve conduction study (NCS) is a method of examining whether a peripheral nerve is performing its main role, that of transmitting electric signals. NCS measures the change of the electric potential obtained as a response after electric stimulation of the nerve from the external medium. The principles of this study are considered to be as follows.

(1) The stimulation current promotes ionic exchange between the internal and the external medium of the axon.

(2) The action potential arises when the local ionic current exceeds the threshold level.

(3) The electric potential produced by many nerve fibers is compounded and measured as the change of the electric potential at the outside of the nerve.

The measured electric potential is considered to express the organic and functional characteristics of the nerve fibers comprising the nerve.

In pathologic nerves, occasionally the amplitude of the electric potential is small. Significant causes include an increased excitation threshold of the nerve fibers, changes in the amplitude and conduction velocity of the action potential of the individual nerve fiber due to contraction and demyelination of the nerve fibers, and a decreased number of nerve fibers [1–3]. However, at present it is difficult to identify which of these phenomena has occurred from the measured electric potential. Computational simulation is a useful method of understanding and classifying these phenomena.

Many simulations of the action potential of a nerve fiber use values of 2 to 4 Ω-m for the resistivity of the extracellular tissues [4–10]. These are representative values of the resistivity of neural tissues [11, 12]. Human peripheral nerves contain tissues with resistivities of 2 to 100 Ω-m [13], which are surrounded by fat and muscle tissue. However, it is less usual to assume these values in simulations [14, 15]. Quantifying the effect of the resistivity of the surrounding tissues on the excitation threshold of nerve fibers is useful in understanding the compound action potentials measured in nerve conduction studies.

Demyelination is one of the most typical organic changes of nerve fibers in neurological disorders involving thin or broken myelin sheaths. In a pathological nerve, the stimulation current intensity required to produce compound action potentials increases and the conduction velocity of the compound action potential decreases. Demyelination is

considered to be one of the causes of these phenomena. Therefore, in this study, we focused on the resistivity of the extracellular tissues and on demyelination in order to investigate the excitation threshold of nerve fiber by performing a simulation of electrical stimulation of the fiber.

2. Electrical Stimulation of a Nerve Fiber

2.1 Model of a myelinated nerve fiber

A myelinated nerve fiber is composed of an axon and its covering myelin sheaths. The myelin sheaths are separated by the nodes of Ranvier at regular intervals. The ionic currents between the internal and external media of the axon at these sites produce temporal and local electrical potential differences, whose conduction transmits electrical signals. The mechanism is expressed in electric circuit form in Fig. 1 [7, 16]. The ionic currents at the nodes of Ranvier are expressed as a few parallel-connected electromotive forces produced by different ionic channels. If we assume that an axon has a constant conductance G_a, the nerve fiber can be modeled as a concatenated structure of nodes of Ranvier connected by G_a.

The myelin sheaths are laminated with membranes a few nanometers thick. Although the axon faces the extracellular fluid at only the nodes of Ranvier in Fig. 1, because the myelin sheath is not a complete insulator, an enhanced model considering leakage at these locations has been proposed [17].

Figure 2 shows the equivalent circuit considering the conductivity of myelin sheaths. The number of lamellar layers n_l is expressed as

$$n_l = 30 \ln \left\{ \frac{\pi (d \times 10^6)^2}{4} \right\} + 10 \qquad (1)$$

where δ is the axonal diameter [18].

The electrical conductivity G_m and capacitance C_m of the myelin sheaths are expressed as

$$G_m = \pi d L (g_l / 2n_l) \qquad (2)$$

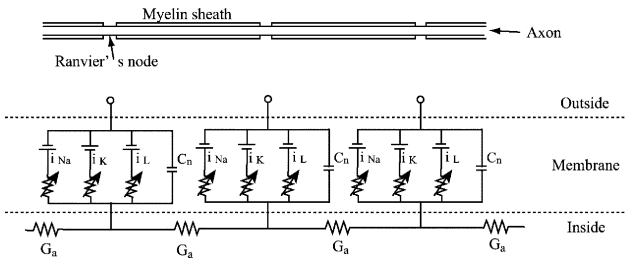

Fig. 1. Myelinated nerve fiber expressed as an electric circuit.

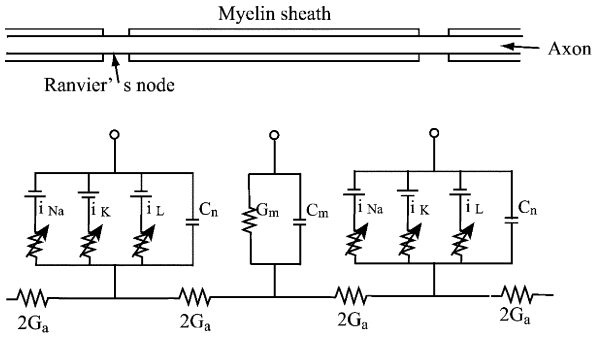

Fig. 2. Myelinated nerve fiber with conductive myelin sheath expressed as an electric circuit.

$$C_m = \pi d L (c_l / 2n_l) \qquad (3)$$

where L is the width of the myelin sheath (i.e., the internodal distance), and g_l and c_l are the electrical conductivity and the capacitance per unit area in a single side of a lamellar sheet (Table A.2).

2.2 Electrical stimulation of myelinated nerve fiber

Local application of an electrical potential difference above a certain level both within and outside the membranes generates an electromotive force at the nodes of Ranvier. Electrical stimulation acts to induce an electromotive force coercively by producing local above-threshold potential differences across the membrane.

Once an electromotive force is generated at a node of Ranvier, it induces an EMF at the adjacent nodes, although

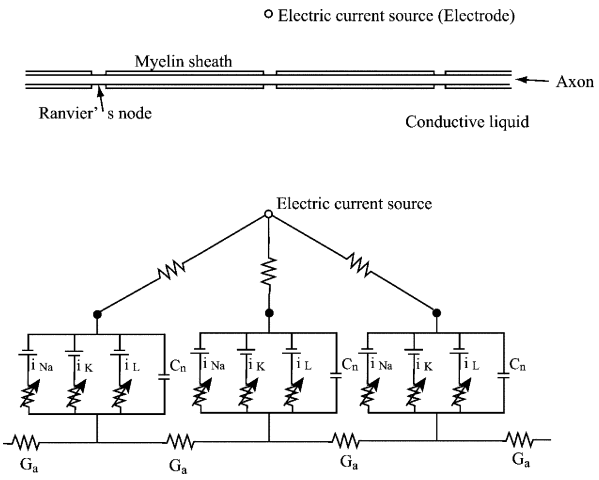

Fig. 3. Electric model of a nerve fiber during stimulation.

the original electromotive force decays over time. This structure permits the nerve fiber to conduct pulse waves (action potentials).

The equivalent circuit of the electrical stimulation of nerve fibers from the external tissues can be expressed as shown in Fig. 3. The stimulation current I can be modeled as the diffusion of an inflow from an infinitesimal stimulation electrode. The expression for the electrical potential V_e at either a node of Ranvier or the myelin sheath will be [7]

$$V_e = \frac{\rho_e I}{4\pi r} \tag{4}$$

where ρ_e is the electrical resistivity of the extracellular tissues, and r is the distance from the point current source to the node of Ranvier or the myelin sheath [7].

3. Simulation of the Electrical Stimulation of a Nerve Fiber

Using such a model of a myelinated nerve fiber, we performed a simulation of the electrical stimulation of nerve fibers that differed in the electrical resistivity of the extracellular tissues and the thickness of the myelin sheath. The constants employed in the model of the node of Ranvier assumed a human sural nerve [19] at 37 °C. The relationship between the outside diameter of the nerve fiber D and the axonal diameter δ, or between D and the internodal length L, followed Wesselink's model, based on measurements by Behse [20, 21]. Here,

$$d = C_d D - D_d \tag{5}$$

$$L = C_L \ln(D/D_L) \tag{6}$$

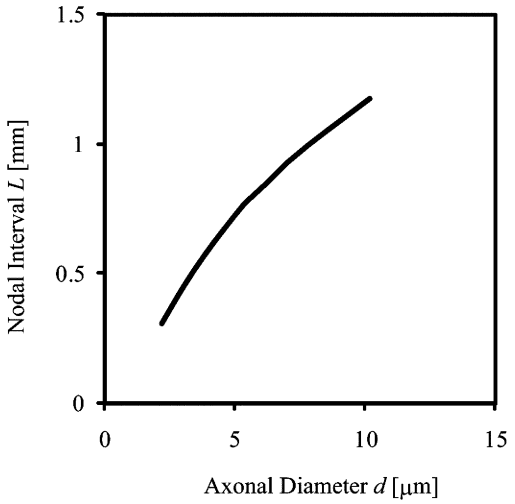

Fig. 4. The relationship between the diameter of the axon and the interval of the Ranvier's nodes of a nerve fiber.

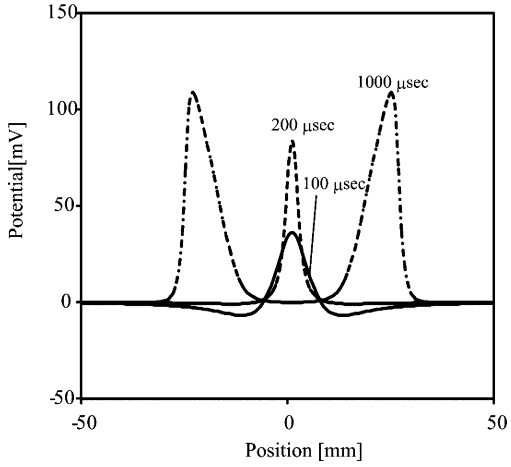

Fig. 5. An example of the action potential of a nerve fiber after stimulation.

The coefficients are expressed in Table A.2. The relationship between δ and L is plotted in Fig. 4.

The nerve fibers were assumed to be stimulated by a point current source in a homogeneous conductor. The point current source was located on a plane containing the perpendicular cross section of a 100-mm-long nerve fiber at its midpoint, which also includes either a node of Ranvier or the center of a myelin sheath. The response after electrical current block pulse stimulation of 100 μs duration was analyzed, with the distance from the current source to the nearest node of Ranvier being varied from 0.1 mm to 10 mm in steps of 0.1 mm. The plots shown in Fig. 5 provide an example of the electric potential distribution after a relatively strong stimulation current above the excitation threshold was applied. In this chart, the numbers next to the waveforms denote the latency. When an action potential arises, the electric potential at the node of Ranvier closest to the current source increases after termination of the stimulation. Consequently, the excitation threshold was defined as the value of the minimum stimulation current which produces a higher electric potential at 200 μs than at 100 μs.

The thickness of the myelin sheaths was defined as n_l, obtained by using Eq. (1), multiplied by the magnification ratio r_l. Here r_l expresses the thickness of the sheath normalized to the standard value. The calculations were performed in the range of 3 Ω-m ≤ ρ_e ≤ 30 Ω-m and 0.2 ≤ r_l ≤ 1.0.

4. Results

Figure 6 shows the relationship between the excitation threshold and the stimulation distance (i.e., the distance

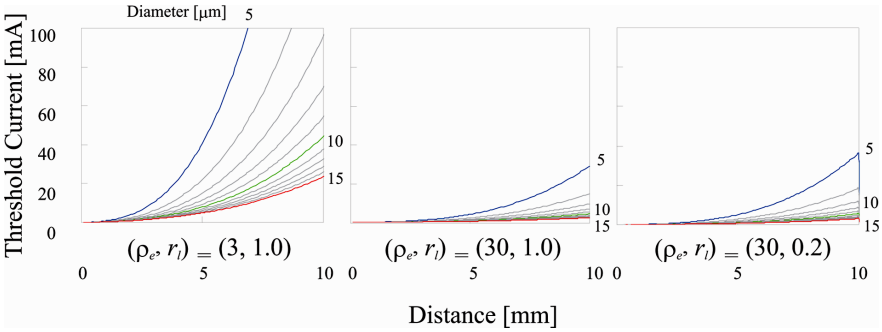

Fig. 6. Calculated threshold current.

from the nerve fiber to the point current source) for different resistivities of the extracellular tissues and thicknesses of the myelin sheaths. The numbers at the top and the right column of the plot areas are the diameters of the nerve fibers. The excitation threshold increased in exponential fashion as the distance of nerve from the stimulation point increased. The excitation threshold increased as the nerve fiber decreased in diameter; for example, when the nerve fiber diameter was 10 μm and 5 μm, the threshold was respectively twice and four times the value for the nerve fiber with 15-μm diameter. This can be regarded as a characteristic behavior of a myelinated nerve fiber stimulated by a monopolar electrode, as indicated by Rattay [22]. This trend was maintained regardless of increases in ρ_e or decreases in r_l.

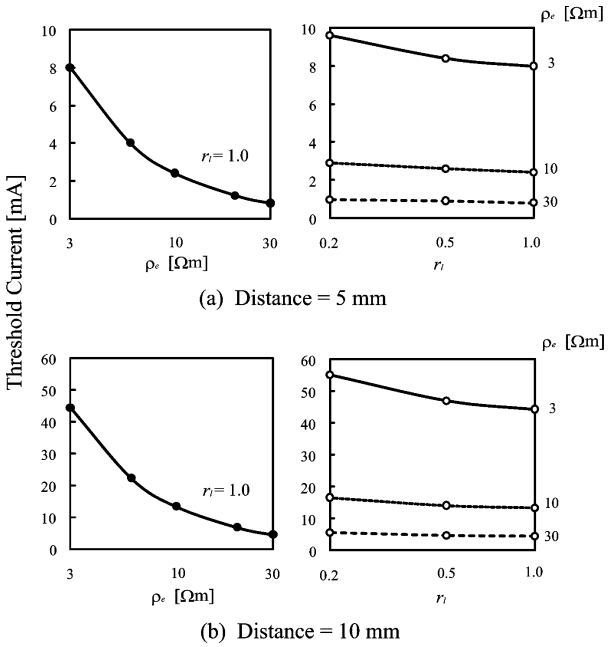

Fig. 7. The threshold current of excitation of a nerve fiber affected by the resistance of the external tissue and the thickness of myelin sheaths.

Both the increase of ρ_e and the decrease of r_l act to boost the excitation threshold. However, the effect of r_l on the excitation threshold was smaller than that of ρ_e. Figure 7 shows the change of the excitation threshold for different ρ_e and r_l with the nerve fiber diameter constant at 10 μm. The curves obtained for stimulation distances of 5 mm and 10 mm are highly similar. The right-hand plots in Fig. 7(a) show that the fluctuation of the excitation threshold is no more than 0.5 mA at ρ_e = 10. The left-hand plots of Fig. 7(a) show that when ρ_e is close to 10, the range of variation of ρ_e corresponding to a 0.5-mA fluctuation of the excitation threshold is 1 to 2 Ω-m.

Similarly, in Fig. 7(b), the variation range of ρ_e corresponding to a 3-mA fluctuation of the excitation threshold is 5 to 6 Ω-m.

5. Discussion

5.1 Effect of the distance from the stimulus point

The excitation threshold increases exponentially with increasing distance of the nerve fiber from the stimulus point. In experimental investigations of myelinated nerve fibers, it has been shown that the excitation threshold of nerve fibers increases exponentially as the distance from the stimulation electrode increases [9, 23]. Such results have been obtained in computer simulations of the peripheral nerves of rabbits [8], but our results confirm the tendency for human nerve fiber models.

5.2 Effects of the thickness of the myelin sheaths

In case of intravital electrical stimulation of the nerve fibers through the external tissues during NCS, changes of resistivity associated with differences in the composition of the tissues surrounding the nerve may change the excitation threshold. Since pathological changes of myelin sheaths

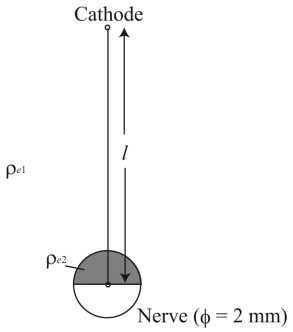

Fig. 8. An example of the situation of nerve stimulation.

such as thinning or defluxion cause the loss of lipids, which form myelin sheaths with high electrical resistivity, the result may be a decrease in the overall resistivity of the external tissues, contributing to an increase in the threshold level.

In Fig. 8 we consider the excitation threshold of a nerve fiber at the core of a cylindrical nerve trunk. Considering the ratio of the axonal diameter to the myelin sheath diameter as 0.7:1, the ratio of the areas of the axon to the myelin sheath in the cross section becomes 1:1. When the resistivities of the axon and the myelin sheath are assumed to be 2 Ω-m and 20 Ω-m, respectively, the resistivity inside the nerve will be approximately 11 Ω-m, that is, the mean of the two resistivities. When l = 5 mm, the mean resistivity between the stimulation point and the nerve fiber is calculated as $0.8\ \rho_{e1} + 0.2\ \rho_{e2}$ = 18.5 Ω-m. If loss of myelin sheaths occurs and ρ_{e2} falls to 2 Ω-m, then the resistivity between the stimulation point and the nerve fiber decreases to 16.4 Ω-m, which is a reduction of about 2 Ω-m from the original value. Our simulation results show that the increase in the threshold is almost the same as that which occurs when the thickness of the myelin sheaths is reduced to 20% of the normal value. This example shows that both a decrease of ρ_e and a decrease of r_l will increase the excitation threshold. Therefore, in addition to demyelination of a nerve fiber itself, demyelination around the nerve fiber may possibly contribute to an increase in the excitation threshold of the nerve fiber.

6. Conclusions

A computer simulation of the electrical stimulation of a nerve fiber in human peripheral nerve from the external tissues was performed as a modeling study of NCS. The results showed that both a decrease of the resistivity of the external tissues and a decrease of the thickness of the myelin sheaths contribute to an increase in the excitation threshold of a nerve fiber.

REFERENCES

1. Bradley JL, Thomas PK, King RHM, Muddle JR, Ward JD, Tesfaye S, Boulton AJM, Tsigos C, Young RJ. Myelinated nerve fibre regeneration in diabetic sensory polyneuropathy: correlation with type of diabetes. Acta Neuropathol 1995;90:403–410.
2. Lindemuth R, Ernzerhof C, Schimrigk K. Comparative morphometry of myelinated nerve fibers in the normal and pathologically altered human sural and tibial nerve. Clin Neuropathol 2002;21:29–34.
3. Llewelyn G, Gilbey SG, Thomas PK, King RHM, Muddle JR, Watkins PJ. Sural nerve morphometry in diabetic autonomic and painful sensory neuropathy. Brain 1991;114:867–892.
4. Abzug C, Maeda M, Peterson BW, Wilson VJ. Cervical branching of lumbar vestibulospinal axons. J Physiol 1974;243:499–522.
5. Andreasen LNS, Struijk JJ, Lawrence S. Measurement of the performance of nerve cuff electrodes for recording. Med Biol Eng Comput 2000;38:447–453.
6. Frijns JUM, ten Kate JH. A model of myelinated nerve fibres for electrical prosthesis design. Med Biol Eng Comput 1994;32:391–398.
7. McNeal DR. Analysis of a model for excitation of myelinated nerve. IEEE Trans Biomed Eng 1976;23:329–337.
8. Rijkhoff NJ, Holsheimer J, Debruyne FMJ, Wijkstra H. Modelling selective activation of small myelinated nerve fibres using a monopolar point electrode. Med Biol Eng Comput 1995;33:762–768.
9. Rubinstein JT. Analytical theory for extracellular electrical stimulation of nerve with focal electrodes. Biophys J 1991;60:538–555.
10. Warman EN, Grill WM, Durand D. Modeling the effects of electric fields on nerve fibres: determination of excitation thresholds. IEEE Trans Biomed Eng 1992;39:1244–1254.
11. Geddes LA, Baker LE. The specific resistance of biological material—a compendium of data for the biomedical engineer and physiologist. Med Biol Eng 1967;5:271–293.
12. Ranck LB. Specific impedance of rabbit cerebral cortex. Exp Neurol 1963;7:144–152.
13. Veltink PH, van Veen BK, Struijk JJ, Holsheimer J, Boom HBK. A modeling study of nerve fascicle stimulation. IEEE Trans Biomed Eng 1989;36:683–692.
14. Altman KW, Plonsey R. Point source nerve bundle stimulation: effects of fiber diameter and depth on simulated excitation. IEEE Trans Biomed Eng 1990;37:688–698.
15. Roth BJ, Altman KW. Steady-state point-source stimulation of a nerve containing axons with an arbi-

trary distribution of diameters. Med Biol Eng Comput 1992;30:103–108.
16. Frijns JHM, Mooij J, ten Kate JH. A quantitative approach to modeling mammalian myelinated nerve fibers for electrical prosthesis design. IEEE Trans Biomed Eng 1994;41:556–566.
17. Blight AR. Computer simulation of action potentials and afterpotentials in mammalian myelinated axons: the case for a lower resistance myelin sheath. Neuroscience 1985;15:13–31.
18. Sugimura K, Dyck PJ. Sural nerve myelin thickness and axis cylinder caliber in human diabetes. Neurology 1981;31:1087–1091.
19. Schwarz JR, Reid G, Bostock H. Action potentials and membrane currents in the human node of Ranvier. Pflügers Arch 1995;430:283–292.
20. Behse F. Morphometric studies on the human sural nerve. Acta Neurol Scand Suppl 132 1990;82:1–38.
21. Wesselink WA, Holsheimer J, Boom HBK. A model of the electrical behaviour of myelinated sensory nerve fibres based on human data. Med Biol Eng Comput 1999;37:228–235.
22. Rattay F. Analysis of models for external stimulation of axons. IEEE Trans Biomed Eng 1986;33:974–977.
23. Bement SL, Ranck JB. A model for electrical stimulation of central myelinated fibers with monopolar electrodes. Exp Neurol 1969;24:171–186.

APPENDIX

Model of Nerve Fiber

Kirchhoff's law:

$$\frac{dV_n}{dt} = \frac{1}{C_m}\{2G_a(V_{e,n-1} + V_{n-1} + V_{e,n+1} + V_{n+1}) + G_m V_e - (4G_a + G_m)V_n\} \text{(for odd n)}$$

$$\frac{dV_n}{dt} = \frac{1}{C_n}(I_{nodal} - I_{ion}) \quad \text{(for even n)}$$

$$G_a = \frac{\pi d^2}{4\rho_i L}$$

$$C_n = c_n \pi d l$$

Table A.1. Gating coefficients

	A [msec^{-1}]	B [mV]	C [mV]
α_m	4.58	-18.4	10.3
β_m	0.329	-22.7	9.16
α_h	0.205	-111	11.0
β_h	14.1	-28.8	13.4
α_n	0.0517	-93.2	1.10
β_n	0.0919	-76.0	10.5

Membrane current (when the subscript n of V is even)

$$I_{nodal} = 2G_a(V_{n-1} - 2V_n + V_{n+1} + V_{e,n-1} - 2V_{e,n} + V_{e,n+1})$$

$$I_{ion} = \pi d l (i_{\mathrm{Na}} + i_{\mathrm{K}} + i_L)$$

$$i_{\mathrm{Na}} = m^3 h P_{\mathrm{Na}} \frac{EF^2}{RT} \frac{(\mathrm{Na})_o - (\mathrm{Na})_i e^{EF/RT}}{1 - e^{EF/RT}}$$

$$i_{\mathrm{K}} = n^4 g_{\mathrm{K}}(V_n - V_{\mathrm{K}})$$

$$i_L = g_L(V_n - V_L)$$

$$E = V_n + V_r$$

Gating

$$m(0) = 0.0382$$

$$h(0) = 0.6986$$

$$n(0) = 0.2563$$

$$dm/dt = \alpha_m(1-m) - \beta_m m$$

$$dh/dt = \alpha_h(1-h) - \beta_h h$$

$$dn/dt = \alpha_n(1-n) - \beta_n n$$

$$\alpha_m = A_{\alpha_m}(V_n - B_{\alpha_m})/(1 - e^{(B_{\alpha_m} - V_n)/C_{\alpha_m}})$$

$$\beta_m = A_{\beta_m}(B_{\beta_m} - V_n)/(1 - e^{(V_n - B_{\beta_m})/C_{\beta_m}})$$

$$\alpha_h = A_{\alpha_h}(B_{\alpha_h} - V_n)/(1 - e^{(V_n - B_{\alpha_h})/C_{\alpha_h}})$$

$$\beta_h = A_{\beta_h}/(1 + e^{(B_{\beta_h} - V_n)/C_{\beta_h}})$$

$$\alpha_n = A_{\alpha_n}(V_n - B_{\alpha_n})/(1 - e^{(B_{\alpha_n} - V_n)/C_{\alpha_n}})$$

$$\beta_n = A_{\beta_n}(B_{\beta_n} - V_n)/(1 - e^{(V_n - B_{\beta_n})/C_{\beta_n}})$$

Table A.2. Constants

C_d	0.8	axon diameter parameter
D_d	1.8 $\times 10^{-6}$ m	axon diameter parameter
C_L	7.9 $\times 10^{-4}$	sheath length parameter
D_L	3.4 $\times 10^{-6}$ m	sheath length parameter
g_l	10 S/m^2	lamella conductivity per unit area
c_l	0.001 F/m^2	lamella capacitance per unit area
ρ_i	0.33 Ω m	axoplasm resistivity
c_n	0.028 μ F/m^2	membrane capacitance per unit area
l	1.5 μm	nodal gap width
F	96514 $\times 10^4$ C/mol	Faraday's constant
R	8.3144 J/K/mol	gas constant
T	310.15	absolute temperature
$(\mathrm{Na})_o$	154 mol/m^3	external sodium concentration
$(\mathrm{Na})_i$	30 mol/m^3	internal sodium concentration
P_{Na}	7.04 $\times 10^{-5}$ m/sec	sodium permeability
g_K	300 S/m^2	potassium conductance
g_L	600 S/m^2	leak conductance
V_K	0 mV	potassium current equilibrium potential
V_L	-0.14 mV	leak current equilibrium potential
V_r	-84 mV	resting potential

AUTHORS (from left to right)

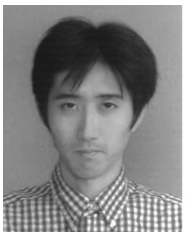

Takehito Hayami (member) received his B.E. and M.E. degrees from the University of Kyushu in 1996 and 1998. He completed the second half of the doctoral program in intelligent systems engineering at the University of Kyushu in 2000 and became a research associate at Hiroshima City University. He became a research associate at the Digital Medicine Initiative, University of Kyushu, in 2006 and an assistant professor in 2007. His research interests are the effects of electromagnetic fields and light on nerves. He holds a D.Eng. degree, and is a member of the Japan Biomedical Society and IEEE.

Keiji Iramina (member) received his B.E. and M.E. degrees from the University of Kyushu in 1986 and 1988. He completed the latter half of the doctoral program in engineering at the University of Kyushu in 1991 and became a research associate there. He was appointed an associate professor in 1994. He moved to the School of Medicine, University of Tokyo, in 1996. In 2004 he became a professor of systems and information at the University of Kyushu. His research interests are functional brain imaging, physiological electromagnetic measurement, and electrical stimulation. He holds a D.Eng. degree, and is a member of the Japan Biomedical Society and IEEE.

Xian Chen (nonmember) completed the doctoral program in mechanical and information engineering at the University of Tokyo in 1994 and became a researcher at the Takasa Research Institute, Mitsubushi Heavy Industries, Ltd. In 1999 he was appointed an associate professor at the University of Tokyo. In 2005 he became a professor at the Digital Medicine Initiative, University of Kyushu. His research interests are computational biomechanics. He holds a D.Eng. degree, and is a member of the JSME and the Japan Biomedical Society.